ARTICLE https://nhsjs.com/

Impact of Electronic Response Parameters on Pulse Shape Discrimination in HPGe Detectors

Nikhil Nanduri

Received August 15, 2025 Accepted October 23, 2025 Electronic access October 31, 2025

Pulse shape discrimination (PSD) is a critical technique for suppressing background events in high-purity germanium (HPGe) detectors. The LEGEND collaboration, in particular, searches for neutrinoless double beta decay $(0v\beta\beta)$ using ⁷⁶Ge detectors. The A/E parameter is frequently used as a method of PSD, showing promising results in the rejection of multi-site, p+, and n+ events. However, a systematic study of how various front-end electronics settings affect this parameter's PSD performance remains lacking. This study addresses this gap by investigating the impact of electronic response parameters on discrimination power. Realistic models of charge-sensitive amplifier responses, low-pass filters, and noise were applied on simulated charge pulses from ²⁰⁸Tl events in ⁷⁶Ge detectors. The effects of these parameters on A/E and pulse shape parameters were then studied. Simulations were implemented using Python with well-established signal processing techniques. Optimal discrimination was observed for low-pass cutoff frequencies near 3-5 MHz. Additionally, excessive filtering and electronic ringing significantly degraded A/E discrimination and the corresponding cut's figure of merit. The triangle filter's rise time and noise amplitude were also found to strongly affect PSD effectiveness. These findings provide additional direction for tuning LEGEND-200 electronics to maximize background rejection. Improved awareness of these dependencies improves event classification and increases sensitivity to rare single-site event signals.

Keywords: Neutrinoless double beta decay, pulse shape discrimination, LEGEND Collaboration, electronic response functions.

1 Introduction

1.1 Background and Motivation

Double beta decay is a rare nuclear process in which a nucleus converts two neutrons into two protons while maintaining its mass number. It occurs in two modes: two-neutrino double beta decay $(2\nu\beta\beta)$, which has been observed experimentally ¹, and neutrinoless double beta decay $(0\nu\beta\beta)$, which has not ².

Discovery of $0\nu\beta\beta$ would confirm the Majorana nature of neutrinos, implying they are their own antiparticles ² and that lepton number is violated. Such a result would have profound implications for the matter–antimatter asymmetry of the universe and the absolute neutrino mass scale, since the decay rate is linked to the effective Majorana mass ^{3–5}.

The physics reach of $0\nu\beta\beta$ searches depends on suppressing backgrounds while retaining signal efficiency. In HPGe detectors, this relies on pulse shape discrimination (PSD), whose performance is set by the readout electronics. Thus, electronics tuning is directly tied to the sensitivity of these experiments.

1.2 Experimental Signatures and Isotope Choices

The experimental signature of $0\nu\beta\beta$ is given by a singular peak at the energy, or Q-value, of the decay on the energy spectrum of the summed electron energies (since the two electrons carry all the decay energy in $0\nu\beta\beta$). This differs from the signature of $2\nu\beta\beta$, which is a spectrum of energy levels resulting from the emission of two antineutrinos that share the available decay energy with the electrons. In recent years, many programs have launched initiatives with the goal of a $0\nu\beta\beta$ observation in isotopes such as $^{76}\text{Ge}^{6.7}$, $^{100}\text{Mo}^{8-10}$, $^{82}\text{Se}^{11,12}$, and $^{130}\text{Te}^{13,14}$. Each isotope has a respective $Q_{\beta\beta}$, which is a crucial consideration in choosing which isotope to potentially observe this process in, as a higher $Q_{\beta\beta}$ typically indicates lower backgrounds.

1.3 The LEGEND Collaboration

The LEGEND (Large Enriched Germanium Experiment for Neutrinoless Double Beta Decay) collaboration searches for $0\nu\beta\beta$ in 76 Ge, with $Q_{\beta\beta}=2039.061$ keV 15,16 . Building on GERDA and MAJORANA DEMONSTRATOR 6,7 , LEGEND proceeds in two phases: LEGEND-200, now operating at LNGS with 200 kg of enriched detectors 17 , and LEGEND-1000, which will scale to 1000 kg 15 . A central challenge is distinguishing

true single-site events (SSE) from gamma-induced multi-site events (MSE), a dominant source of background 18 . Pulse shape discrimination, especially through the A/E parameterthe ratio of maximum current amplitude to total energyremains the primary technique for suppressing MSE 19,20 .

However, the effectiveness of A/E is not intrinsic to the crystal alone but strongly depends on the readout electronics. Variations in charge-sensitive amplifier design, filter cutoff frequencies, shaping times, and noise coupling can distort A/E, shifting thresholds and broadening SSE/MSE distributions. Despite its importance, no systematic study has quantified how these electronic response parameters influence PSD in HPGe detectors. Since LEGENDs sensitivity depends directly on maximizing background rejection while retaining > 85% of SSE, even modest degradation in separation reduces the attainable half-life reach. This work addresses this gap by systematically simulating how electronics response shapes A/E discrimination in LEGEND-style detectors.

1.4 Scope

This study addresses this gap by simulating charge pulses from ⁷⁶Ge double-beta decay events and systematically varying electronic response and signal processing parameters, including low-pass filter cutoff frequency, triangle filter rise time, and noise levels. The effects of these parameters on A/E distributions and pulse shape features are then studied, providing additional information regarding the optimization of electronics settings for maximal event discrimination power in LEGEND and similar experiments.

2 Methods

2.1 Event Data and Signal Construction

For PSD optimization 208 Tl γ rays were used from a 228 Th source. The 2615 keV transition produces the Double Escape Peak (DEP, \sim 1593 keV), Single Escape Peak (SEP, \sim 2103 keV), and Full Energy Peak (FEP, 2615 keV)²¹. DEP events are dominated by single-site energy depositions, while SEP and FEP are enriched in multi-site interactions. This clear contrast provides well-defined samples for training and testing PSD, where the goal is to efficiently retain single-site events while rejecting multi-site backgrounds. A set of simulated ²⁰⁸Tl event waveforms was obtained from prior Monte Carlo studies of energy depositions in LEGEND-200 detectors ²². For each event, the deposited charge as a function of time, $Q_{in}(t)$, was provided. These signals were padded with a zero baseline until 45000 ns, then padded with the maximal charge value to best replicate real signals. The corresponding current waveform was calculated via numerical differentiation, and it can be viewed in Figure 1.

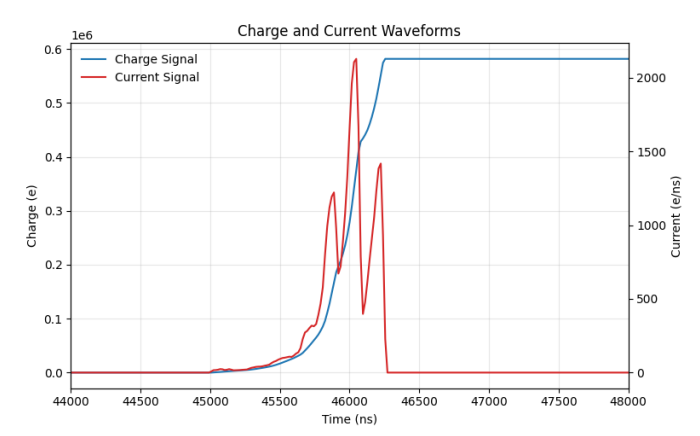


Fig. 1 Example charge deposition signal and derived input current for a single event.

2.2 Detector Impulse Response Functions

To model the detector readout chain, each input current signal was convolved with an impulse response, $h_{\rm CSA}(t)$, representing the front-end charge-sensitive amplifier and associated shaping electronics.

The total response function is the convolution:

$$h_{\text{CSA}}(t) = h_{\text{FB}}(t) * h_{\text{LP}}(t)$$

where $h_{FB}(t)$ is the feedback decay response and $h_{LP}(t)$ is the low-pass filter response.

2.2.0.1 Feedback Decay Response: The feedback network (parallel R_f and C_f) is modeled as a single-pole exponential decay²³:

$$h_{ ext{FB}}(t) = rac{1}{ au_f} e^{-t/ au_f}, \quad ext{for } t \geq 0$$

where $\tau_f = R_f C_f$ is the decay time constant.

Here $\tau_f=3$ ms, which is much longer than the $\sim \! 100$ ns rise time of the signals. This parameter controls the long tail decay of the CSA output, and was chosen to be much longer than the rise time of the signals such that it does not distort short-timescale pulse features and allows the trapezoidal filter to provide an unbiased energy estimate. It essentially acts as a polezero correction, flattening the waveform top so that the trapezoidal filter can provide an unbiased energy estimate.

2.2.0.2 Second-Order Butterworth Low-Pass Response: The dominant signal shaping is modeled by a second-order Butterworth low-pass filter with cutoff frequency f_c^{23} :

$$h_{\mathrm{LP}}(t) = rac{\sqrt{2}}{ au} \sin\left(rac{t}{\sqrt{2} au}
ight) e^{-t/(\sqrt{2} au)}, \quad ext{for } t \geq 0$$

where the shaping time, $\tau = 1/(2\pi f_c)$. This filter was chosen as it provides stronger high-frequency suppression than a

first-order RC while remaining analytically simple for isolating cutoff effects. The typical cutoff frequency incorporated in LEGEND-200 ranges on the order of a few MHz, and is one of the parameters that will be modified in this study. The final impulse response of the CSA is normalized such that it has unit area.

2.3 Waveform Generation and Electronic Noise

The output CSA waveform, $V_{CSA}(t)$, is calculated as:

$$V_{\text{CSA}}(t) = I_{\text{in}}(t) * h_{\text{CSA}}(t)$$

To simulate experimental conditions, additive Gaussian noise with amplitude σ_n was included, with σ_n ranging from 8×10^{-5} to 6×10^{-4} a.u., levels < 1% the CSA waveform's height. This low amplitude reflects the excellent noise performance of HPGe detector electronics, which is essential for achieving superior energy resolution in rare event searches like neutrinoless double-beta decay ¹⁵. Also, a sinusoidal ringing noise term of frequency $f_{\rm ring}$ and amplitude $A_{\rm ring}$ was superimposed to model electronic pickup.

2.4 Digital Filtering and Feature Extraction

To determine the A/E parameter, the energy E for each event was first estimated by applying a digital trapezoidal filter to $V_{\rm CSA}(t)$. The trapezoidal filter estimates the peak of the pulse over a specified shaping interval by averaging the signal and subtracting delayed copies of itself, resulting in a flat-topped output whose maximum value is proportional to the total deposited charge (and thus the energy of the event)²⁴. This requires two parameters: the rise time (how long the filter takes to peak) and the flat-top time (how long the filter stays at its peak), which were chosen to be 4 μ s and 2.5 μ s, respectively. At the sampling step of dt=16 ns, these correspond to L=250 samples and G=156 samples. The trapezoidal filter can be expressed recursively as:

$$\begin{split} Y[k] &= Y[k-1] + x[k] - x[k-L_{\text{trap}}], \\ S_{\text{trap}}[k] &= \frac{1}{L_{\text{trap}}} \big(Y[k] - Y[k-G_{\text{trap}} - L_{\text{trap}}] \big) \end{split}$$

where x[k] is the discrete CSA waveform, Y[k] is the running sum over the last L samples (boxcar integrator), $L_{\rm trap}$ is the rise (or integration) time, and $G_{\rm trap}$ is the flat-top (or gap) time 21 . The FIR kernel is equivalent to the difference of two length-L boxcars separated by G samples.

A triangular filter was then applied on the trapezoidal filter's output to extract the shaped value of the maximal current amplitude, A. This method is often used in experiments to approximate the point-to-point derivative of the CSA output. The triangle filter is mathematically equivalent to a trapezoidal filter with no flat top time, acting as a finite difference operator²⁴. For

the triangular filter, the rise length was varied from $L_{\rm tri} = 1$ to 15 samples (16240 ns).

The recursion was implemented as:

$$T[k] = T[k-1] + S[k] - S[k-2L_{\mathrm{tri}}]$$

$$S_{\text{tri}}[k] = \frac{T[k]}{2L_{\text{tri}}}$$

This corresponds to convolution with a symmetric triangular kernel of width $2L_{\rm tri}$. The rise time of the triangle filter ideally should be as short as possible, being 1 sample (or 16 ns) for the best approximation of a derivative. However, the effect of noise on the triangle filter output is amplified with a shorter rise time, causing an eventual trade-off for a larger rise time at high-enough noise levels.

Figure 2 shows both the trapezoidal and triangle filters when applied to a CSA output. The peak of each of these filters is then extracted, with the peak of the triangle filter (A) being divided by the peak of the trapezoidal filter (E) to finally determine the A/E parameter for an event.

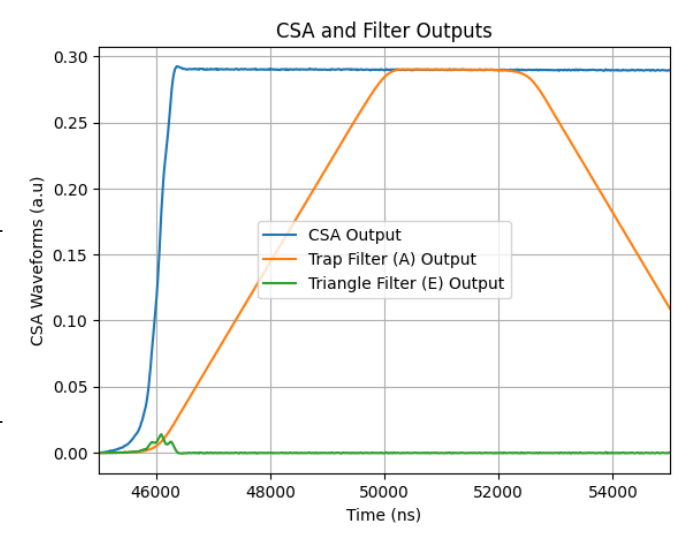


Fig. 2 Application of trapezoidal and triangle filters to the CSA output.

2.5 A/E Distribution and Pulse Shape Discrimination

The A/E value has been frequently used as a method of pulse shape discrimination since it is systematically lower for MSE when compared to SSE^{18,19}. This occurs because MSE pulses rise more slowly and are spread out in time, reducing the peak value measured by the triangle filter relative to the pulses total energy. As such, when an A/E histogram was constructed for large ensembles ($N \sim 193,000$) of simulated events, it's expected that the histogram sees a sharp peak at a higher value representing the peak of the SSE distribution. Figure 3 shows the generated distribution, which forms the basis for event selection.

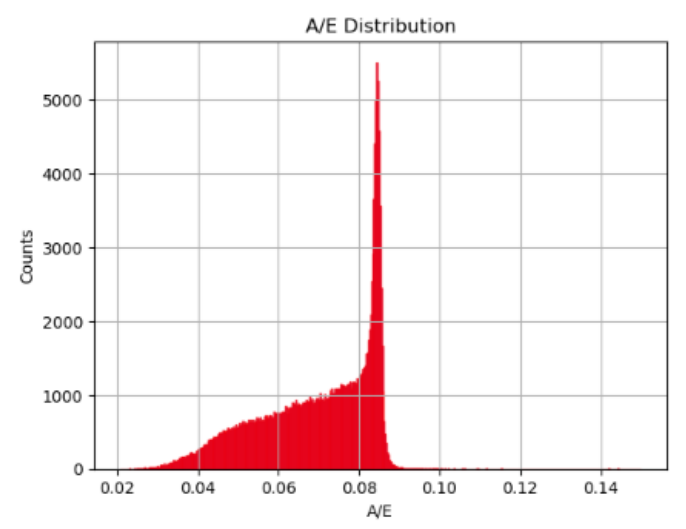


Fig. 3 Histogram of A/E values for all simulated events. A/E peak corresponds to high number of SSE at that value.

2.6 Event Classification and Energy Resolution

DEP/SEP/FEP events were classified directly from the true deposited energies in the Monte Carlo, yielding distinct peaks without overlap from other γ lines. For Tl-208, these categories correspond to energy depositions at approximately 1593 keV (DEP), 2102 keV (SEP), and 2615 keV (FEP), respectively 21 . DEP events are predominantly single-site (SSE), whereas SEP and FEP events are primarily multi-site (MSE) due to the involvement of annihilation photons. This allows the use of energy deposition as an accuracy metric of the A/E discrimination power while certain parameters are changed. Figure 4 shows the classification of events based on their energy deposition. These peaks can be ignored for the purposes of this study, as the focus lies on event-based discrimination using only the DEP, SEP, and FEP regions.

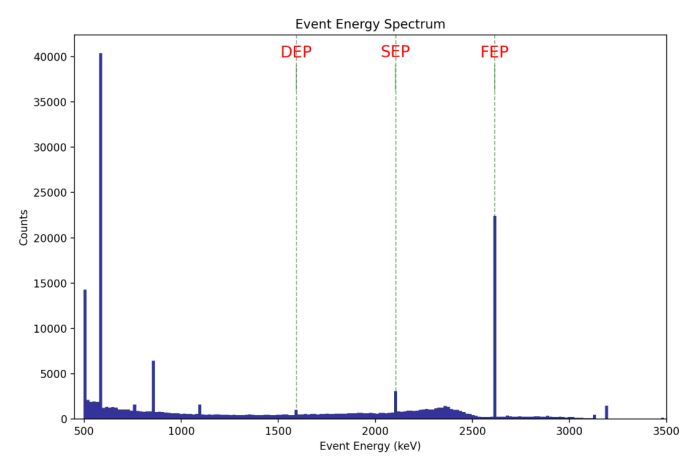


Fig. 4 Simulated energy spectrum after classification, showing DEP, SEP, and FEP event populations.

2.7 Figure of Merit Determination and Optimization

Once the energy deposition spectrum was created, an energy mask of ± 5 keV was produced around the DEP, SEP, and FEP peaks to fully capture the peaks and minimize contamination from other lines and fully isolate SSE/MSE events. The ± 5 keV energy window is wide enough to contain all simulated peak populations, while remaining narrow enough to suppress contributions from the surrounding Compton continuum and unrelated events. Table 1 summarizes the sensitivity of events counted for each mask width.

Peak	$\pm 2~\mathrm{keV}$	$\pm 5~\mathrm{keV}$	$\pm 10~\mathrm{keV}$
DEP	582	793	1142
SEP	2436	2791	3285
FEP	21232	22312	22473

Table 1 Event counts within ± 2 , ± 5 , and ± 10 keV selection windows for DEP, SEP, and FEP.

Additional peaks in the spectrum arise from other gamma-ray emissions of Tl-208, as well as other annihilation processes within the detector. Figure 5 shows the resulting A/E histogram when all other energy events are filtered and each event is properly classified. There is quite a significant overlap between the A/E values of SSE and MSE events, so this study also investigates factors that would help reduce this overlap and therefore better signal discrimination.

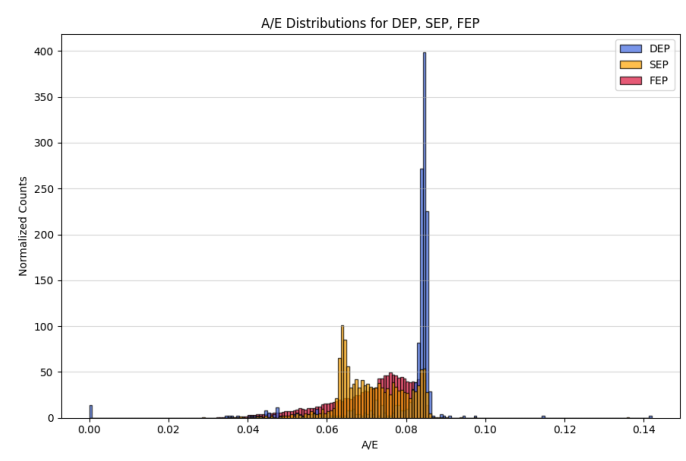


Fig. 5 Event-based A/E histogram.

A commonly used Figure of Merit (FoM)in PSD studies was used to quantify how well the DEP/SSE events were discriminated from background/MSE events, given by:

$$FoM = \frac{Signal\ Acceptance}{\sqrt{Background\ Acceptance}}$$

where signal acceptance corresponds to the fraction of DEP events retained after an A/E cut (eliminating all events greater

than a certain A/E value), and background acceptance to the fraction of SEP and FEP events that survived the A/E threshold. This formula is widely used in the context of rare-event searches 25 .

Other formulas were also tried, but this expression provided the most reasonable signal acceptance while keeping the background acceptance relatively low. A higher FoM indicates better event discrimination, with the overall goal of PSD to maximize the FoM. For each set of parameters, various A/E cuts were iterated, providing an optimization curve as seen in Figure 6. A minimum signal acceptance of 0.85 was implemented to ensure that the FoM was not too heavily weighted by an unnecessarily small background acceptance. This aligns with typical values used in LEGEND, which aims for 90% signal efficiency and 5-10% background efficiency 15 . The maximal FoM value was then compared across different sets of parameter values, with the greatest FoM value among those being ideal.

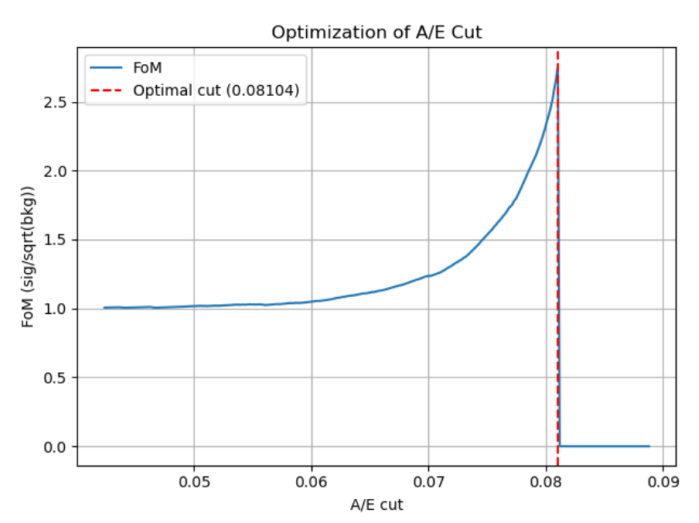


Fig. 6 Example FoM optimization for different A/E cuts.

A full range of parameters tested in this study can be found in Table 2.

Parameter	Range	Step size
f_c	1.0 – 10.0 MHz	0.1 MHz
$L_{ m tri}$	16 - 240 ns	16 ns
$L_{\rm trap}$	$4 \mu s$	fixed
$G_{ m trap}$	2.5 μs	fixed
$\sigma_{ m noise}$	$0,5 \times 10^{-6} - 5 \times 10^{-2}$	decade steps
$A_{ m ring}$	0.009 a.u.	fixed
$f_{ m ring}$	0 - 3.6 MHz	0.025 MHz

Table 2 Parameter scan ranges and step sizes used in this study.

3 Results

3.1 CSA Overshoot

Varying the low-pass filter cutoff frequency significantly alters the pulse shape characteristics and the A/E distribution. One noticeable aspect of the CSA waveform was the initial overshoot peak. When testing different parameters' effects on this overshoot, the low-pass filter's cutoff frequency exacerbated this occurrence with lower cutoff frequencies. Figure 7 shows the CSA outputs for varying cutoff frequencies, and Figure 8 quantifies the median of this overshoot for different types of events. For example, DEP overshoot decreases from about 3% at 1 MHz to below 1% at 10 MHz, with SEP and FEP following the same trend. The uncertainties on these medians are <0.1% and do not affect the observed monotonic trend.

The overshoot is shown to be systematically greater for SSE (DEP events) compared to MSE (SEP and FEP events). This is expected because the low-pass filter is less capable of keeping up with the rapid and steep rise of single-site events, resulting in a more pronounced overshoot. In contrast, multi-site events typically produce slower pulses, which are less affected by the filter's limited response time. Since there is a noticeable effect of the low-pass filter on the overshoot, the effects of this parameter on the FoM were then studied as the overshoot potentially modifies the value of A/E.

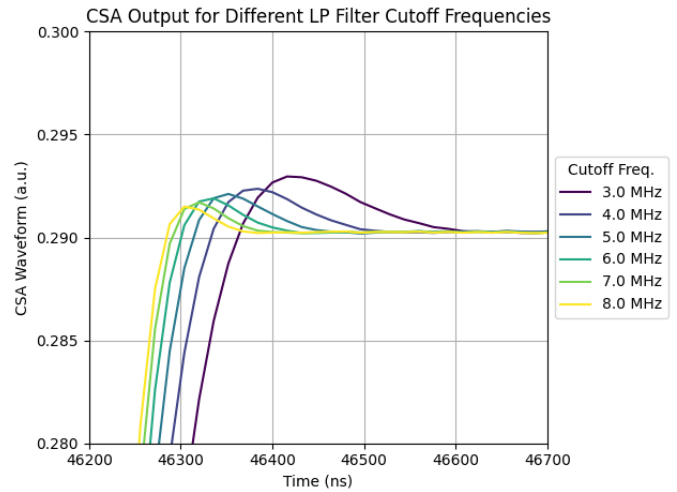


Fig. 7 Differing CSA outputs when varying low-pass filter cutoff frequency.

3.2 Impact of Low-Pass Filter Cutoff Frequency

For each different cutoff frequency, an A/E histogram, like the one in Figure 5, was produced. The A/E median for each type of event (DEP, SEP, and FEP) was then measured and plotted against cutoff frequency, as seen by Figure 9. A greater differ-

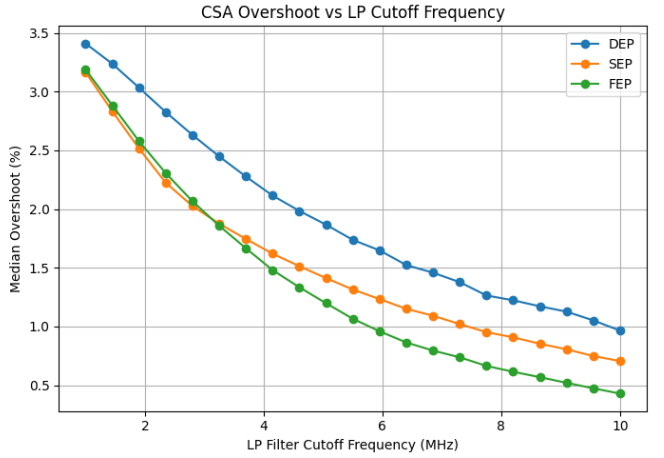


Fig. 8 CSA Overshoot (calculated as percent increase from trapezoidal filter output) for different cutoff frequencies and event types.

ence between SSE and MSE medians indicates better discrimination between the two events, and it appears this difference is optimized past approximately 5 MHz. A FoM analysis was then conducted with this same variable to produce Figure 10, yielding two distinct peaks near 3 MHz and 5.4 MHz.

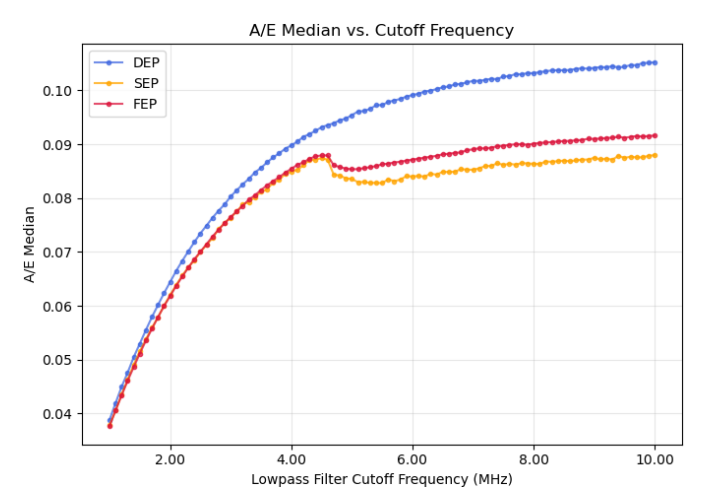


Fig. 9 A/E median for different cutoff frequencies while simultaneously manipulating the type of event.

These optimal values arise because lower cutoff frequencies stretch out the fast SSE pulses and reduce the extracted peak current A, while higher cutoffs transmit additional high-frequency components that broaden the A/E distribution. The MHz-scale maxima therefore reflect the balance between preserving SSE edge sharpness and limiting waveform distortion. To validate the findings from the FoM analysis, a plot of signal efficiency vs. cutoff frequency was incorporated at a fixed background acceptance of 7.5%, yielding Figure 11.

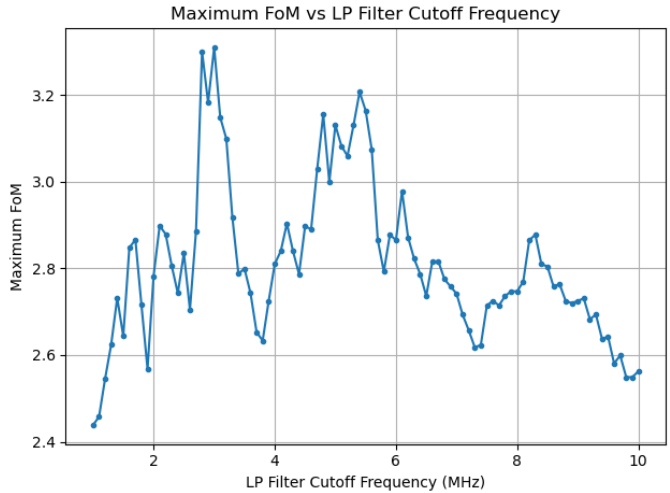


Fig. 10 Signal and background acceptance FoM for different cutoff frequencies.

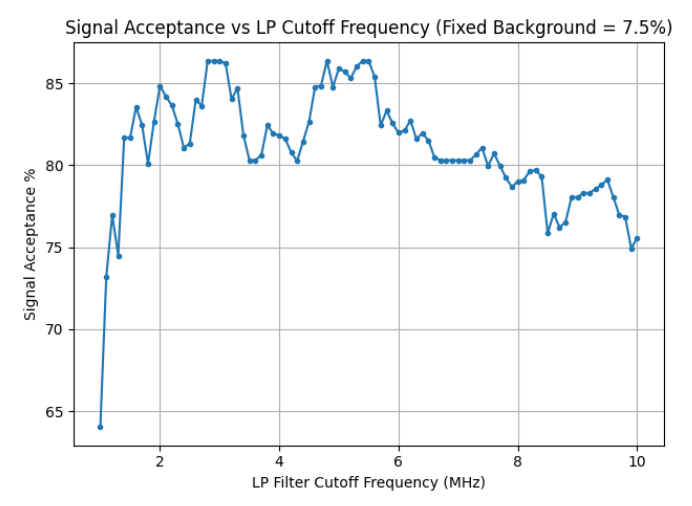


Fig. 11 Signal acceptance as a function of LP Filter Cutoff Frequency.

3.3 Triangle Filter Rise Time Optimization

Acting as a point-to-point derivative of the CSA output with a rise time of only 1 sample (16 ns), a triangle filter's rise time - under the presence of no noise - should ideally always be as short as possible. However, under the presence of noise, there's a balance that must be achieved: very short rise times act like near point-to-point derivatives, which maximize sensitivity to SSE edges but also make the output highly sensitive to random noise. Longer rise times suppress those fluctuations by averaging over more samples, but at the cost of smearing the true peak current A. The observed maximum FoM then reflects the compromise between noise averaging and signal fidelity, and that tradeoff can be viewed in Figure 12.

Table 3 demonstrates how noise (amplitude represents standard deviation of gaussian-appproximated noise) degrades PSD

performance, but a further study should be conducted into mea- oscillations, capturing the main frequency and amplitude of the suring realistic noise from HPGe detectors and providing a standardized model of the varying sources.

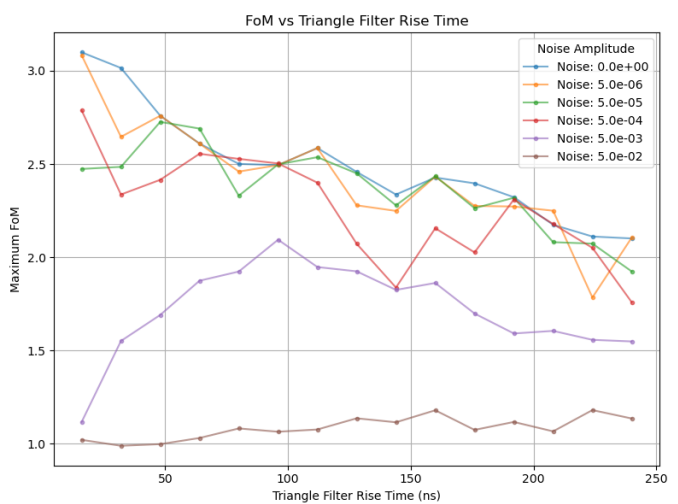


Fig. 12 FoM as a function of triangle filter rise time, for several noise levels.

Noise Amplitude	Best FoM	Rise Time (ns)
0	3.0991	16
5e-6	3.0833	16
5e-5	2.7262	48
5e-4	2.7877	16
5e-3	2.0946	96
5e-2	1.1811	224

Table 3 Best FoM and corresponding triangle filter rise time for each tested noise amplitude.

Ringing Response Function

Oscillatory (ringing) features in the output response of HPGe charge-sensitive amplifiers can arise from under damped electronic response functions, parasitic circuit resonances, orin some casespickup of high-frequency (MHz) noise from external sources. To model this, a sinusoidal ringing term with variable frequency and amplitude was added to the CSA long-tail feedback response function, given by:

$$h_{\rm ring}(t) = e^{-t/\tau_1} + A_{\rm ring} e^{-t/\tau_2} \sin\left(2\pi f_{\rm ring} t\right)$$

where τ_1 is the main decay constant (3 ms), τ_2 is the damping time of the ringing (50 μ s), A_{ring} is the amplitude of the oscillatory term (0.009 a.u.), and f_{ring} is the ringing frequency. The sinusoidal model reflects how underdamped circuits and external MHz pickup appear in HPGe electronics as damped

ringing without modeling full circuit complexity.

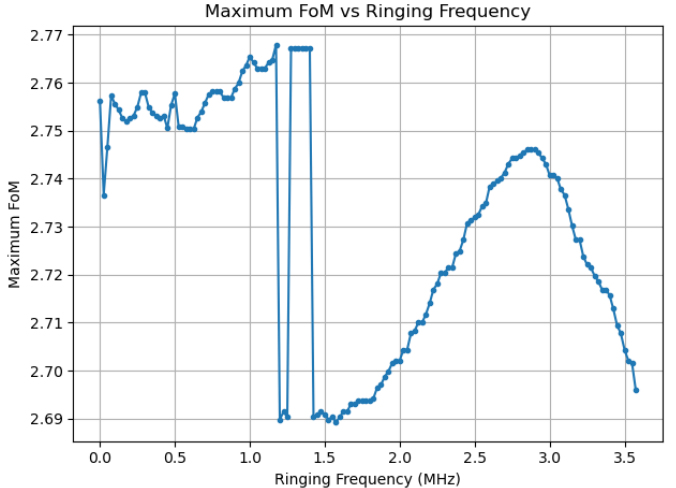


Fig. 13 Varying ringing response function frequency effect on the A/E

Discussion

Summary of Main Results

This study systematically investigated how variations in electronic response parameters including low-pass filter cutoff frequency, triangle filter rise time, and simulated electronic ringingaffect the performance of pulse shape discrimination (PSD) in LEGEND-200 HPGe detector signals. Errors on signal and background acceptance were estimated by counting statistics, using the standard formula $\sigma = \sqrt{\frac{p(1-p)}{N}}$, where *p* is the measured fraction, and *N* is the number of events. Typical statistical uncertainties were about 13% due to the large number of events sampled. Using Monte Carlo simulations of ²⁰⁸Tl events, the following key results were obtained:

- Novel observation of CSA overshoot: A systematic overshoot in the CSA output tail was observed when lowering the low-pass filter cutoff frequency, most pronounced for SSE events. The overshoot magnitude increased at lower bandwidths, especially for rapid-rising SSE signals, and diminished at higher cutoffs. This effect directly altered the A/E distribution and, by extension, discrimination power.
- Discrimination power maximized at MHz-scale cutoffs: The Figure of Merit (FoM) for A/E-based PSD was maximized at low-pass filter cutoff frequencies above 5 MHz, with two broad peaks observed around 3 MHz and 5.4 MHz. The FoM increased by up to 40% relative to sub-MHz settings. This relative increase corresponds to nearly a factorof-two reduction in surviving background acceptance at

fixed signal efficiency (e.g., at 85% SSE acceptance, MSE leakage is reduced by approximately 50%). Thus, even small relative improvements in FoM have a significant practical impact on PSD performance.

- Triangle filter rise time: The PSD performance depended sensitively on the rise time of the triangle filter. Optimal FoM values of 16 and 48 ns were found for noise levels similar to those in HPGe detectors.
- Impact of electronic ringing: Simulating a damped, sinusoidal ringing term in the CSA response revealed that ringing frequencies near 12 MHz led to a significant broadening of the A/E distribution and a ~25% reduction in FoM. This illustrates the real risk posed by electronic pickup and mechanical coupling at specific frequencies, which can substantially undermine PSD effectiveness if not properly controlled.
- Sensitivity to shaping vs. noise: Across all tested scenarios, the tuning of electronic response functions (shaping, filtering, and ringing mitigation) had a greater impact on event discrimination than moderate variations in baseline noise amplitude. At very large, unrealistic noise amplitudes (≥ 5 × 10⁻⁴ a.u.), Table 3 shows that PSD performance degrades sharply; however, within the realistic LEGEND regime (≤ 10⁻⁵ a.u.), shaping and ringing parameters remain the dominant factors.

Parameter	FoM Range	% Change
$f_c (110 \text{ MHz})$	1.9 - 3.1	+63%
$L_{\rm tri} \ (16240 \ {\rm ns})$	1.2 - 3.1	+158%
$\sigma_n (5 \times 10^{-6} - 5 \times 10^{-2})$	1.2 - 3.1	+160%
$f_{\rm ring}$ (03.6 MHz)	2.3 - 3.1	+35%

Table 4 Sensitivity of the Figure of Merit (FoM) to each tested parameter. Ranges correspond to the minimum and maximum FoM observed across the scanned interval. Percentage change is computed as $(FoM_{max} - FoM_{min})/FoM_{min} \times 100\%$.

4.2 Interpretation and Physical Implications

The observed dependence of PSD performance on filter parameters can be attributed to the interplay between signal bandwidth, electronic noise, and pulse shape characteristics. Short triangle filter rise times enable more precise extraction of the current peak but are more susceptible to noise, explaining the observed degradation in FoM at higher noise levels. The optimal low-pass cutoff arises from the need to preserve fast signal features while minimizing noise amplification. Ringing introduces oscillatory distortions that broaden the A/E distribution, worsening signal discrimination power.

4.3 Implications for LEGEND-200 and PSD Optimization

The results indicate that achieving optimal PSD in LEGEND-200 depends heavily on fine-tuning the electronic shaping parameters to maximize signal-to-noise and minimize the impact of both baseline noise and high-frequency interference. Careful control of filter cutoffs, amplifier response, and shielding against external noise is critical, as suboptimal settings or excess pickup at MHz frequencies can substantially degrade event discrimination. While the A/E variable remains an effective PSD tool under well-optimized electronics, its robustness diminishes quickly when shaping or filtering parameters drift from their optimal range.

4.4 Limitations

Several limitations must be noted. First, the analysis is based on Monte Carlo simulated events and idealized detector geometry. Effects like charge trapping and cloud charges were not included in these simulations. The effects of cloud charges would further smear the A/E distribution due to cloud charge repulsion and diffusion. The noise model used is also simplified and may not reflect the true spectral composition of noise sources in experimental setups. Also, the detector response function was only an approximation that simplified the incredibly complex electronics makeup of HPGe detectors. There is currently not a widely standardized response function for these detectors, as it is an ongoing work of study.

4.5 Future Work

Future efforts should focus on incorporating measured noise traces from operating HPGe detectors to develop a more realistic noise model. Additionally, investigating a more accurate response function using circuit analysis of the LEGEND-200 CSA would be incredibly valuable. Further studies could also explore the impact of these variables on the alternative late-charge (LQ) PSD parameter⁶. Incorporating sideband subtraction to improve the classification of DEP/SEP/FEP events is also recommended. Finally, future studies should include parasitic capacitances and inductances in their electronic models to assess their impact on PSD performance.

4.6 Conclusion

In summary, this work demonstrates the sensitivity of A/E-based PSD and pulse shape features, to the details of electronic response in HPGe detectors. The findings provide actionable guidance for electronics optimization in LEGEND-200 and similar experiments, emphasizing the need for careful control of noise, filter parameters, and pickup mitigation to achieve maximal background rejection and sensitivity to rare event signals.

Acknowledgments

This research wouldn't have been possible without the crucial support and guidance of Dr. Reyco Henning and the entire Experimental Nuclear and Astroparticle Physics (ENAP) Group at UNC Chapel Hill.

References

- 1 S. R. Elliott, A. A. Hahn and M. K. Moe, Direct evidence for two-neutrino doublebeta decay in 82Se, 2008, https://doi.org/ 10.1103/PhysRevLett.59.2020.
- 2 E. Majorana, *Teoria simmetrica dell'elettrone e del positrone*, 1937, https://doi.org/10.1007/BF02961314.
- 3 M. Fukugita and T. Yanagida, *Baryogenesis without grand unification*, 1986, https://doi.org/10.1016/0370-2693(86)91126-3.
- 4 M. Agostini, G. Benato, J. A. Detwiler, J. Menendez and F. Vissani, *Toward the discovery of matter creation with neutrinoless decay*, 2023, https://doi.org/10.1103/RevModPhys.95.025002.
- 5 J. Schechter and J. W. F. Valle, Neutrinoless double- decay in SU(2)U(1) theories, 1982.
- 6 MAJORANA Collaboration, Final Result of the MAJORANA DEMON-STRATOR's Search for Neutrinoless Double- Decay in 76Ge, 2023, https: //doi.org/10.1103/PhysRevLett.130.062501.
- 7 GERDA Collaboration, Final Results of GERDA on the Search for Neutrinoless Double- Decay, 2020, https://doi.org/10.1103/PhysRevLett.125.252502.
- 8 AMoRE Collaboration, Improved Limit on Neutrinoless Double Beta Decay of 100Mo from AMoRE-I, 2025, https://doi.org/10.1103/PhysRevLett.134.082501.
- 9 CUPID Collaboration, Final results on the 0 decay half-life limit of 100Mo from the CUPID-Mo experiment, 2022, https://doi.org/10.1140/epjc/s10052-022-10942-5.
- 10 NEMO Collaboration, Results of the search for neutrinoless double-decay in 100Mo with the NEMO-3 experiment, 2015, https://doi.org/10.1103/PhysRevD.92.072011.
- 11 CUPID Collaboration, Final Result on the Neutrinoless Double Beta Decay of 82Se with CUPID-0, 2022, https://doi.org/10.1103/ PhysRevLett.129.111801.
- 12 NEMO Collaboration, *Final results on 82Se double beta decay to the ground state of 82Kr from the NEMO-3 experiment*, 2018, https://doi.org/10.1140/epjc/s10052-018-6295-x.
- 13 CUORE Collaboration, With or without? Hunting for the seed of the matter-antimatter asymmetry, 2024, https://doi.org/10.48550/ arXiv.2404.04453.
- 14 CUORE Collaboration, Search for Majorana neutrinos exploiting millikelvin cryogenics with CUORE, 2022, https://doi.org/10.1038/ s41586-022-04497-4.
- 15 LEGEND Collaboration, The Large Enriched Germanium Experiment for Neutrinoless Decay: LEGEND-1000 Preconceptual Design Report, 2021, https://doi.org/10.48550/arXiv.2107.11462.

- 16 B. J. Mount, M. Redshaw and E. G. Myers, Double- decay Q-values of 74Se and 76Ge, 2010.
- 17 L. Baudis, G. Benato, E. M. Bond, P. J. Chiu, S. R. Elliott, R. Massarczyk, S. J. Meijer and Y. Muller, *Calibration sources for the LEGEND-200 ex*periment, 2023, https://doi.org/10.1088/1748-0221/18/02/ P02001.
- 18 GERDA Collaboration, Modeling of GERDA Phase II data, 2020, https://doi.org/10.1007/JHEP03(2020)139.
- 19 GERDA Collaboration, Pulse shape analysis in Gerda Phase II, 2022, https://doi.org/10.1140/epjc/s10052-022-10163-w.
- 20 MAJORANA Collaboration, Multisite event discrimination for the MAJORANA Demonstrator, 2019, https://doi.org/10.1103/ PhysRevC.99.065501.
- 21 G. F. Knoll, Radiation Detection and Measurement, 4th Ed., 2010.
- 22 S. Giri, Emulating PSD Parameters using IQN, Pulse Shape Simulation Workshop, University of Zurich, 2010.
- 23 S. Butterworth, On the Theory of Filter Amplifiers, 1930.
- 24 V. Radeka, Trapezoidal Filtering of Signals from Large Germanium Detectors at High Rates, 1972, https://doi.org/10.1109/TNS.1972.4326542.
- 25 S. P. MacMullin, Elastic and inelastic scattering of neutrons from neon and argon: Impact on neutrinoless double-beta decay and dark matter experimental programs, 2013, https://doi.org/10.17615/1bgsyt67, Ph.D. thesis.

Supplementary Information

Data and Code Availability

The Jupyter notebook containing all simulation and analysis code, as well as a representative HDF5 event file, are available in a public GitHub https://github.com/nikhil135790/Impactof-Electronic-Response-Parameters-on-Pulse-Shape-Discrimination.ipynb.

Implementation Details

Simulations were implemented in Python (version 3.10). Numerical computation was performed with NumPy, HDF5 event files were read with h5py, and filtering operations were carried out using scipy.signal. Joblib was used for parallelization, and select routines were accelerated with the Numba just-in-time compiler. Visualization and figure generation employed Matplotlib.